Real-Time Autodetachment Dynamics of Vibrational Feshbach Resonances in a Dipole-Bound State

Do Hyung Kang, Sejun An, and Sang Kyu Kim[*]
Department of Chemistry, KAIST, Daejeon 34141, Republic of Korea

Feshbach resonances corresponding to metastable vibrational states of the dipole-bound state (DBS) have been interrogated in real time for the first time. The state-specific autodetachment rates of the DBS of the phenoxide anion in the cryogenically cooled ion trap have been directly measured, giving $\tau \sim 33.5$ ps for the lifetime of the most prominent $11'^1$ mode (519 cm^{-1}). Overall, the lifetime of the individual DBS state is strongly mode dependent to give $\tau \sim 5$ ps for the $18'^1$ mode (632 cm^{-1}) and $\tau \sim 12$ ps for the $11'^2$ mode (1036 cm^{-1}). The qualitative trend of the experiment could be successfully explained by the Fermi's golden rule. Autodetachment of the $11'^1 18'^1$ combination mode is found to be much accelerated ($\tau \leq 1.4$ ps) than expected, and its bifurcation dynamics into either the $11^1 18^0$ or $11^0 18^1$ state of the neutral core radical, according to the propensity rule of $\Delta v = -1$, could be distinctly differentiated through the photoelectron images to provide the unprecedented deep insights into the interaction between electronic and nuclear dynamics of the DBS, challenging the most sophisticated theoretical calculations.

Since first conceived by Fermi and Teller in 1947 [1], the dipole bound state (DBS) has been the subject of the intensive investigation [2–5]. Even though the electron is only loosely bound, a variety of processes such as electron transfer [6,7], isomerization [8], or dissociation [9,10] take place in the frame of DBS. It also plays a crucial role as a doorway state in the electron-capture process in the interstellar medium or biological environments [11,12]. The electron transfer is often associated with the weakly bound electrons for efficient signal and energy transfers [13]. Therefore, an understanding the DBS is indispensable for thorough description of the electron transfer.

From the perspective of the anion, the vertical transition to the neutral radical is direct and instantaneous. This is the transition from the bound to the continuum, and the photodetachment efficiency behaves according to the Wigner's threshold law ($\sigma_{\text{detachment}} \propto \sqrt{eKE}$). However, when the DBS exists, the indirect process mediated by the bound-to-metastable DBS transitions occurs. This gives rise to vibrational Feshbach resonances corresponding to the DBS vibrational states [14,15]. Although the energetic structures of DBS could be informed from the photodetachment spectroscopy [16], its temporal dynamics has remained yet to be resolved as the line shape analysis, except for some unusual cases [17,18], is intrinsically nontrivial. Femtosecond time-resolved photoelectron spectroscopy has been extremely valuable to get the direct picture of the DBS dynamics [19–21]. And yet, as the energetic window of the femtosecond laser is so wide, it seems that the state-specific real-time dynamics of DBS is hitherto unrealized yet.

Herein, phenoxide (PhO$^-$) is a target system. Phenoxide is ubiquitous and its role in many important chemical and biological processes has been intensively studied [22,23]. Energetics involved in the photodetachment of PhO$^-$ have been well established, giving the electron affinity (EA) of 2.253 eV and $+0.952$ eV for the appearance of the first excited PhO [24–26]. The structural change upon the photodetachment has been reflected in the vibrational structure of the photoelectron spectrum, giving the most prominent progression of the ν_{11} mode. The recent spectroscopic work for the cryogenically cooled PhO$^-$, pioneered by the Wang group [27,28], has provided well-resolved DBS vibrational structures above the detachment threshold. Accordingly, the electron binding energy has been precisely estimated to be 97 cm^{-1}, and the vibrational structures of the neutral core could be determined by the photoelectron images.

In this Letter, we report the first state-specific, real-time dynamics of the vibrational DBS Feshbach resonances of the PhO$^-$ prepared in the cryogenically cooled ion trap, using the picosecond pump-probe time-resolved photoelectron velocity-map imaging method [29–31]. As we have employed the cryogenically cooled ion trap [32,33], the rotational temperature of the PhO$^-$ anion is maintained at $T_{\text{rot}} \sim 35$ K [34]. This minimizes the rotational effect on the dephasing of DBS while it sharpens the resonance bandwidth [35], making it possible to isolate only one specific vibrational DBS at a time within the energetic window ($\Delta\nu \sim 20$ cm^{-1}) of the laser pulse. In the time-resolved velocity-map electron imaging setup, vibrational structures of the neutral core resulting from direct or
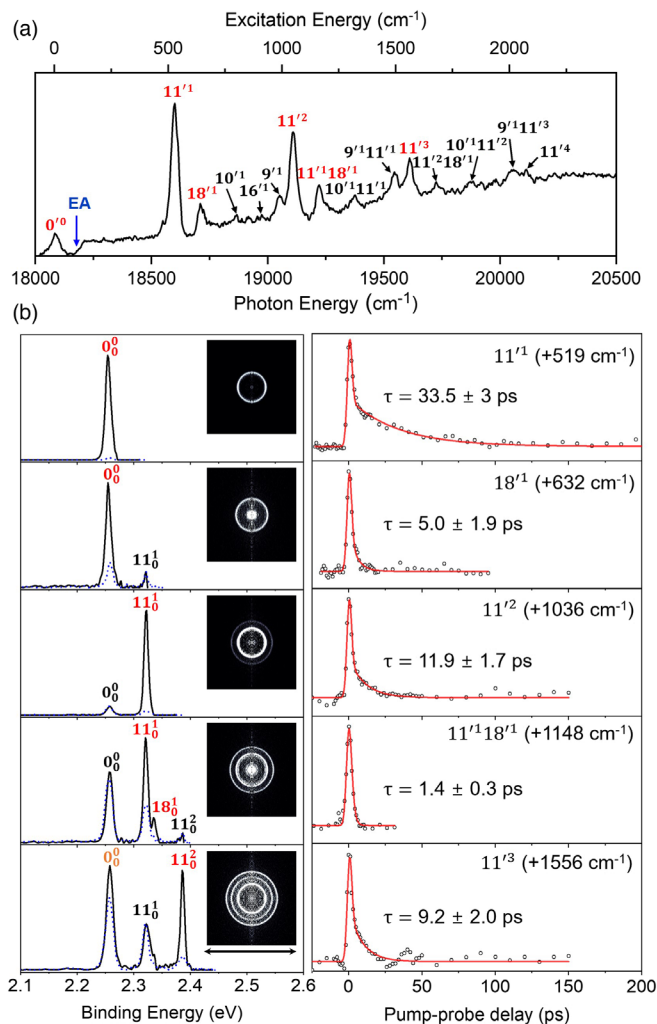
FIG. 1. (a) Picosecond photodetachment spectrum of the phenoxide (PhO⁻) anion. The time-resolved photoelectron images have been taken for the peaks denoted by the assignments in red. (b) Photoelectron images and time-resolved transients of the phenoxide DBS resonances for five selected bands of $11'^1$ ($+519$ cm^{-1}), $18'^1$ ($+632$ cm^{-1}), $11'^2$ ($+1036$ cm^{-1}), $11'^1 18'^1$ ($+1148$ cm^{-1}), and $11'^3$ ($+1556$ cm^{-1}). (Left) Photoelectron spectra and (inset) corresponding photoelectron images. Photoelectron spectra taken at the off-the-resonance positions near the resonance energies represent the nonresonant direct photodetachment (the blue dotted lines). At each DBS resonance, the photoelectron spectrum shows the large signal enhancement at the particular vibrational levels (labeled in red) according to the propensity rule of $\Delta v = -1$. The peak showing the small enhancement of the signal by the resonance excitation is labelled in orange, and this could be attributed to the vibronic coupling. The polarization axis of the picosecond laser is shown as the black arrow. (Right) Photoelectron transients have been fitted to get the time constants for the single exponential decay functions (see the Supplemental Material [36]). The intensity axes were reversed in order to show the population decay of the vibrational Feshbach resonances.

indirect photodetachment could be unambiguously differentiated in both frequency and time domains. This uniquely combined experimental setup is extremely useful for unraveling the nonadiabatic coupling dynamics of the DBS. The autodetachment rate is found to be strongly mode dependent in terms of its internal energy and the nature of nuclear displacements. Especially, as both the rate and branching ratio could be simultaneously determined for the combination mode, the bifurcation dynamics of individual Feshbach resonances into different product states could be unambiguously identified, giving the deep insights into the nonadiabatic coupling mechanism.

In Fig. 1(a), the photodetachment spectrum of the cryogenically cooled phenoxide anion is taken by monitoring the total photoelectron yield as a function of the wavelength of the picosecond laser pulse ($\Delta t \sim 1.7$ ps, $\Delta \nu \sim 20$ cm^{-1}). Sharp resonances are clearly observed on the top of the broad structureless background signal emerging from the detachment threshold of 18 173 cm^{-1}. Except the broad bandwidths, the photodetachment spectrum of PhO⁻ is quite consistent with that reported from the Wang group, which was obtained by the nanosecond laser pulse [27]. The ν_{11} progression stands out, reflecting the structural change upon the photodetachment. The ν_{18} mode and its combination with the ν_{11} progression are also quite notable. Resonances become weakened and obscure in the high energy region, whereas the background intensity increases with increasing the photon energy, Fig. 1(a). A resonance band observed below the photodetachment threshold is due to the transition to the zero-point energy level of the DBS ($0'^0$) [27]. Obviously, as the $0'^0$ state lies below the electron affinity (EA) threshold, the lifetime of the DBS ground state is expected to be quite long. When the photodetachment spectrum is taken with the additional picosecond laser pulse of 791 nm after the delay time of 40 ps, only the $0'^0$ band intensity shows the large enhancement, whereas the other whole spectral features remain same (see the Supplemental Material [36]). This indicates that only the long-surviving $0'^0$ state gets the additional photon at the delay time of 40 ps. Photoelectron velocity-map images taken at the DBS peaks represent the vibrational distributions of the neutral core radical produced from direct and/or indirect photodetachment [Fig. 1(b)]. For the direct process, the Franck-Condon (FC) factors dictate the vibrational distributions whereas the propensity rule of $\Delta v = -1$ is rather strictly obeyed in the autodetachment from the DBS [16,37]. The contribution of the nonresonant direct photodetachment seems to be quite pronounced in the photoelectron images taken by the picosecond laser pulse presumably because of its different nature both in temporal and/or energetic bandwidths [38].

The picosecond time-resolved photoelectron images are taken for the lifetime measurements of the DBS vibrational states. In order to obtain transients, the pump and probe

scheme has been employed. By the finely tuned pump laser pulse, the PhO$^-$ anion gets excited to a specific DBS; whereas the probe laser pulse at 791 nm depopulates the excited DBS to the detachment continuum, which leads to the high kinetic energy electron emission. The time delay between the pump and probe laser pulses is varied, giving the transients reflecting the DBS lifetime. For the $0'^0$ band, the transient is taken by monitoring the total photoelectron as a function of the delay time (see the Supplemental Material [36]). The $0'^0$ transient shows the rapid rise at the time zero while it remains intact within ∼500 ps, indicating that its lifetime is at least longer than tens of nanosecond [39].

The transient of the $11'^1$ DBS at $E_{int} = 519$ cm^{-1} has been taken by monitoring only the low-kinetic energy portion of the photoelectron by masking the outer part of the phosphor screen. The probe laser pulse, when it is applied within the lifetime of the particular DBS, would depopulate the excited DBS to diminish the intensity of the slow photoelectron signal coming from the autodetachment of DBS. On the other hand, the depopulation of the DBS by the probe generates the photoelectron in the high kinetic energy region. And thus, the total photoelectron signal in the pump-probe scheme would not reflect the DBS lifetime. One can avoid such a cancellation and unravel the real-time dynamics of the DBS by monitoring the photoelectron signal in the low-kinetic energy region originating from the autodetachment of the metastable Feshbach resonances. The resultant $11'^1$ transient shows a sharp feature at the time zero, which is followed by the relatively slow recovery of the signal [Fig. 1(b)]. The sharp feature may correspond to the coherent spike that originates from the multiphoton processes, including the strong-field effect, as the perfectly spatiotemporally overlapped pump and probe laser pulses at the time zero depopulate the $11'^1$ level most efficiently by any means. This spike survives only during the cross-correlation width of two laser pulses. The subsequent recovery of the photoelectron signal then represents the exponential decay of the DBS due to the autodetachment. The fit to the experiment gives the lifetime (τ) of 33.5 ± 3.0 ps for the $11'^1$ band, which is much longer than previously predicted from the spectral analysis [35]. This is the first real-time measurement of the DBS autodetachment rate in a state-specific way. It is notable that it is generally consistent with the vibrational autodetachment rates previously reported for different molecular systems in terms of the order of magnitude in the timescale [19,21]. In this regard, we have measured the lifetimes of additional vibrational resonances by the same method. Remarkably, the $18'^1$ transient at $E_{int} = 632$ cm^{-1} gives the much shorter lifetime of 5.0 ± 1.9 ps. The sixfold increase of the autodetachment rate of $18'^1$ compared to that of $11'^1$ is quite dramatic as the energy difference between $18'^1$ and $11'^1$ is only 113 cm^{-1}. The mode effect is confirmed by the lifetime measurement of the $11'^2$ band at 1036 cm^{-1}, giving $\tau = 11.9 \pm 1.7$ ps. It is continuously observed in
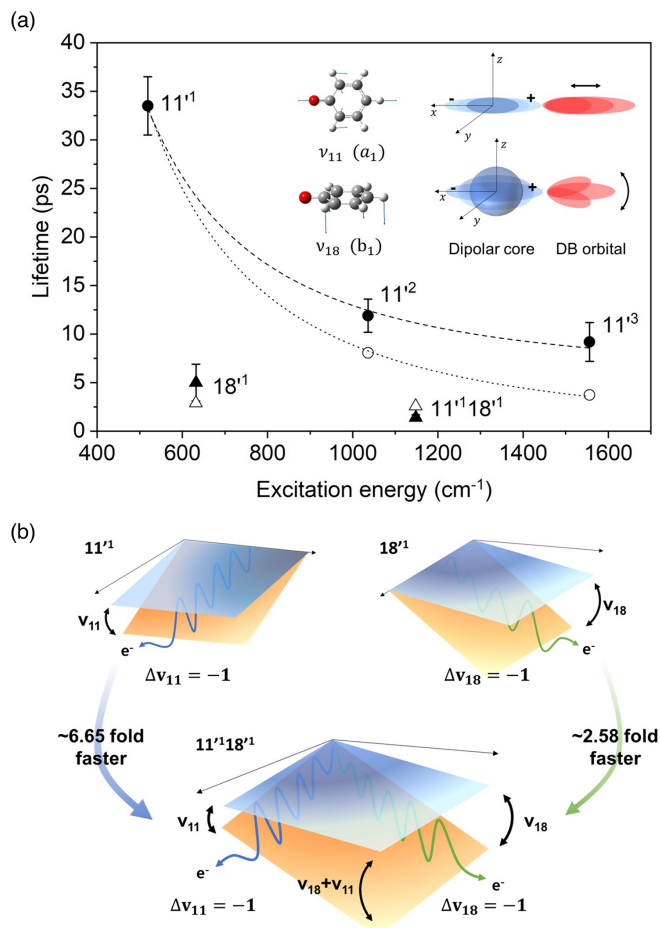

FIG. 2. (a) State-specific lifetimes of the vibrational Feshbach resonances of the phenoxide DBS. Experimentally measured (filled) and calculated (open) lifetimes of the v_{11} (circle) and v_{18}-containing (triangle) vibrational modes are depicted. Normal-mode of the v_{11} and v_{18} and the schematics of the "wobbling" dipole-bound orbital by the relevant vibrational modes were described in the inset. Inverse of a second-order polynomial of the E_{int} was used as a fit function for the experiment (dashed) and calculation (dotted) for v_{11} modes (see the text) as a visual guide. (b) Schematic diagram of the autodetachment process of the $11'^1 18'^1$ combination mode (below) compared to that of the $11'^1$ or $18'^1$ mode (top), respectively. Autodetachment induced by the $\Delta v_{11} = -1$ (blue arrow) or $\Delta v_{18} = -1$ (green arrow) is depicted.

the $11'^3$ transient taken at $E_{int} = 1556$ cm^{-1}, giving $\tau = 9.2 \pm 2.0$ ps. The $11'^1 18'^1$ DBS transient taken at $E_{int} = 1148$ cm^{-1} gives an even faster autodetachment rate, giving $\tau = 1.4 \pm 0.3$ ps as an upper limit (see Figs. 1 and 2). Intriguingly, it is possible to differentiate two distinct autodetachment channels of the $11'^1 18'^1$ mode dephasing into two different product quantum states of $11^1 18^0$ or $11^0 18^1$ mode of the neutral core radical. The branching ratio of the $11^1 18^0$ to the $11^0 18^1$ product has been estimated to be ∼2.6 from the comparison of the photoelectron images taken at the combinational resonance with those taken at the off-resonance excitation [Fig. 1(b)].

TABLE I. Experimentally measured (left) and calculated (right) terms of the Eq. (1) for each vibrational mode (see text).

	Experimentally measured					Calculated		
Transition	eKE (cm^{-1})	ϵ_{if} (cm^{-1})	Coupling const (cm^{-1})	DOS ($\times 10^{21}$ J^{-1})	k^{-1} (ps)	$\partial\mu/\partial Q$ (arb. unit)[a, b]	Coupling const[a]	k^{-1} (ps)
$11'^1 \rightarrow 0_0^0$	422	519	0.98	1.31	33.5	1	1	33.5
$11'^2 \rightarrow 11_0^1$	420	517	1.65	1.31	11.9	...	2.01	8.4
$11'^3 \rightarrow 11_0^2$	424	521	1.88	1.31	9.2	...	2.99	3.8
$18'^1 \rightarrow 0_0^0$	535	632	2.40	1.48	5.0	4.11	3.38	2.6
$11'^1 18'^1 \rightarrow 18_0^1$	419	516	...	1.31	1.4	1	1.01	2.4
$11'^1 18'^1 \rightarrow 11_0^1$	532	629	...	1.47		4.11	3.39	

[a]Relative constants normalized with respect to the value for the $11'^1 \rightarrow 0_0^0$ transition.
[b]Derived from the phenoxyl radical IR intensity calculation using B3LYP/6-311++g(d, p) (Fig. S8).

Although the quantitative analysis of the present experiment seems to be formidable, the Fermi's golden rule could be invoked [39,40] for the interpretation.

$$k = \frac{2\pi}{\hbar} |\langle \phi_f | W | \phi_i \rangle|^2 \rho(E) \quad (1)$$

Here, ϕ_i and ϕ_f are the initial and final states, respectively, W is the coupling operator between the two states, and ρ is the density of states (DOS) of the ejecting electron, where E is its kinetic energy.

$$\rho(E) = \frac{V}{2\pi^2} \left(\frac{2m_e}{\hbar^2} \right)^{\frac{3}{2}} E^{\frac{1}{2}}. \quad (2)$$

V is the orbital volume. From the charge-dipole interaction potential, the most probable radius of the orbital could be estimated to be 31.8 Å (see the Supplemental Material [36]) [39]. And then, from the measured rates in Eq. (1), one can experimentally deduce the coupling constant (σ), $|\langle \phi_f | W | \phi_i \rangle|$. As anticipated from measured rates, σ $(11'^2)$, σ $(11'^3)$, or σ $(18'^1)$ is ~1.65, 1.88, or 2.40 cm^{-1}, respectively, Table I.

Absolute values of the coupling constants are difficult to estimate, and yet their relative ones could be predicted from the theoretical analysis of the Fermi's golden rule [40,41] as follows.

$$\langle \phi_f | W | \phi_i \rangle = -\frac{\hbar^2}{2m} \langle v_f | F(Q) \frac{\partial}{\partial Q} | v_i \rangle \quad (3)$$

$$F(Q) = \frac{1}{\epsilon_{if}} \langle e_f | \left(\frac{\partial U}{\partial Q} \right) | e_i \rangle \quad (4)$$

Here, Q is the normal mode coordinate and ϵ_{if} is the change in the nuclear kinetic energy upon the vibrational autodetachment [42]. For DBS, the potential energy (U) derivative with respect to Q, $(\partial U/\partial Q)$, should be proportional to $\partial\mu/\partial Q$ as U is proportional to the dipole moment (μ) [43,44]. The infrared absorption cross section

of PhO is calculated to be ~16.9 times larger for the ν_{18} mode compared to that of the ν_{11} (see the Supplemental Material [36]). As the IR intensity is proportional to $(\partial\mu/\partial Q)^2$, the relative ratio of σ $(18'^1)$ to σ $(11'^1)$ is then predicted to be 3.38. This successfully explains the much shorter lifetime of 5.0 ps for the $18'^1$ mode compared to that of the $11'^1$ mode, although the even shorter lifetime of 2.4 ps for the $18'^1$ mode is anticipated from theory when the theoretical values were normalized to the experimental lifetime of the $11'^1$ state, Table I. From the perspective of the physical model based on the "wobbling" of the oscillating dipoles [40], the present experiment may sound counterintuitive as the dipole oscillation due to ν_{18} (b_1) is towards the perpendicular (z axis) direction whereas that of ν_{11} (a_1) is parallel to the charge-dipole interaction plane (xy plane), see Fig. 2. However, as the "wobbling" along the z axis of the $18'$ mode strongly influences the dipole moment change along the xy plane, the simple one-dimensional physical model may not be satisfactory. Rather, the overall three-dimensional dynamic change of the charge distribution should be considered.

For the $11'^2$ and $11'^3$ DBS, according to the propensity rule of $\Delta v = -1$, the vibrational motion responsible for the electron detachment is one quantum of the 11 mode. In this case, $F(Q)$ in the Eq. (4) is likely to be unmodified from that of the $11'^1$ mode whereas the derivative vibrational FC factor, $\langle v_f | (\partial/\partial Q) | v_i \rangle$, should be strongly influenced by the different initial and final vibrational quantum numbers. Assuming the Hermite-Gaussian function for the vibrational wave functions (see the Supplemental Material [36]), due to the derivative recurrence of the Hermite polynomial,

$$\frac{\partial}{\partial Q} H_n(Q) = 2n H_{n-1}(Q), \quad (5)$$

Eq. (3) gives the FC derivative integral, which is proportional to the vibrational quantum number of the initial state (n). The resultant relative coupling constants give the autodetachment rate with the relative ratio of 4.0 or 8.9

for the $11'^2$ and $11'^3$ DBS, respectively, compared to that of the $11'^1$ state. This is qualitatively consistent with the experiment, Table I, suggesting that the increase of the autodetachment rate for the overtone DBS originates from the increase of the derivative FC coupling term. According to the Eq. (5), the autodetachment rate is then approximately proportional to the square of the initial vibrational quantum number (n^2), see Fig. 2.

If the simple kinetic relation is applied to estimate the autodetachment rate from the measured rates of the individual $11'^1$ and $18'^1$ modes, the lifetime of the $11'^1 18'^1$ DBS is expected to be ~ 4.4 ps ($k_{11'^1} + k_{18'^1}$). This is much longer than the experimental value of $\tau \leq 1.4$ ps. Furthermore, the branching ratio into the $11^1 18^0$ to $11^0 18^1$ state is supposed to be ~ 6.7, according to the measured ($k_{18'^1}/k_{11'^1}$) ratio. It is much larger than the experimentally estimated branching ratio of 2.6 from the resonant-photoelectron image [Fig. 1(b)]. This discrepancy strongly indicates that the autodetachment from the $11'^1 18'^1$ combination mode cannot be described by the simple addition of two independent kinetic processes. In order to fulfill both the rate and branching ratio, the autodetachment rate from the $11'^1 18'^1$ DBS into $11^1 18^0$ or $11^0 18^1$ state should be ~ 2.58 or ~ 6.65 times faster than that of the $18'^1$ or $11'^1$ fundamental mode, respectively ($k_{11'^1 18'^1 \rightarrow 11^1} = 2.58 k_{18'^1}$, $k_{11'^1 18'^1 \rightarrow 18^1} = 6.65 k_{11'^1}$). This indicates that two vibrational motions of the combination mode should cooperatively speed up the overall autodetachment process even though the quantum selection rule enforces the final quantum state to be distinctly different in the asymptotic limit. One can imagine the electron placed on the two-dimensional plate as depicted in Fig. 2(b). Upon the combination mode excitation, both of two different ways of "wobbling" of the plate are activated to make the electron to fall from the plate, much more efficiently compared to the case of the single mode excitation where the only one directional "wobbling" is turned on. From the relatively larger enhancement in the rate of the $11'^1 18'^1$ DBS into the $11^0 18^1$ state compared to that of the $11^1 18^0$ state, the dynamic cooperative role of the $18'$ mode in the autodetachment process leading to the $11^0 18^1$ state seems to be much more efficient than the case of the other way around. The sophisticated dynamic calculations are quite desirable for understanding this very interesting experimental finding.

In summary, dynamics of the DBS vibrational Feshbach resonances have been unraveled in real time in a state-specific way for the first time by employing the picosecond time-resolved pump-probe scheme. The autodetachment rate of the DBS of the phenoxide anion in the cryogenically cooled ion trap is found to be strongly mode-dependent in terms of the structural fluctuation induced by the normal mode excitation. Particularly, bifurcation dynamics in the autodetachment from the DBS combination mode into different final product quantum states could be distinctly differentiated through the picosecond time-resolved photoelectron images, giving the deep insights into the interaction between electronic and nuclear dynamics of DBS. This work will be extremely helpful for the understanding of the DBS in terms of its structural and dynamical aspects of the interplay between electronic and nuclear motions, motivating lots of high-level theoretical calculations. The current experimental approach could be extended to other nonvalence anions such as quadrupole- [45] or correlation-bound state [46].

*Corresponding author.
 sangkyukim@kaist.ac.kr
[1] E. Fermi and E. Teller, Phys. Rev. **72**, 399 (1947).
[2] K. D. Jordan and F. Wang, Annu. Rev. Phys. Chem. **54**, 367 (2003).
[3] J. Simons, Annu. Rev. Phys. Chem. **62**, 107 (2011).
[4] T.-C. Jagau, K. B. Bravaya, and A. I. Krylov, Annu. Rev. Phys. Chem. **68**, 525 (2017).
[5] G.-Z. Zhu and L.-S. Wang, Chem. Sci. **10**, 9409 (2019).
[6] S. B. King, A. B. Stephansen, Y. Yokoi, M. A. Yandell, A. Kunin, T. Takayanagi, and D. M. Neumark, J. Chem. Phys. **143**, 024312 (2015).
[7] E. Matthews, R. Cercola, G. Mensa-Bonsu, D. M. Neumark, and C. E. H. Dessent, J. Chem. Phys. **148**, 084304 (2018).
[8] Y. Albeck, K. G. Lunny, Y. Benitez, A. J. Shin, D. Strasser, and R. E. Continetti, Angew. Chem. Int. Ed. **58**, 5312 (2019).
[9] W.-L. Li, A. Kunin, E. Matthews, N. Yoshikawa, C. E. H. Dessent, and D. M. Neumark, J. Chem. Phys. **145**, 044319 (2016).
[10] A. Kunin, W.-L. Li, and D. M. Neumark, Phys. Chem. Chem. Phys. **18**, 33226 (2016).
[11] A. Kunin and D. M. Neumark, Phys. Chem. Chem. Phys. **21**, 7239 (2019).
[12] P. D. Burrow, G. A. Gallup, A. M. Scheer, S. Denifl, S. Ptasinska, T. Märk, and P. Scheier, J. Chem. Phys. **124**, 124310 (2006).
[13] J. P. Rogers, C. S. Anstoter, and J. R. R. Verlet, Nat. Chem. **10**, 341 (2018).
[14] M. Tulej, F. Guthe, M. V. Pachkov, K. Tikhomirov, R. Xu, M. Jungen, and J. P. Maier, Phys. Chem. Chem. Phys. **3**, 4674 (2001).
[15] C. E. H. Dessent, J. Kim, and M. A. Johnson, Faraday Discuss. **115**, 395 (2000).
[16] D. M. Wetzel and J. I. Brauman, J. Chem. Phys. **90**, 68 (1989).
[17] T. Pino, M. Pachkov, M. Tulej, R. Xu, M. Jungen, and J. P. Maier, Mol. Phys. **102**, 1881 (2004).
[18] F. Guthe, M. Tulej, M. V. Pachkov, and J. P. Maier, Astrophys. J. **555**, 466 (2001).
[19] J. N. Bull, C. S. Anstöter, and J. R. R. Verlet, Nat. Commun. **10**, 5820 (2019).

[20] M. A. Yandell, S. B. King, and D. M. Neumark, J. Am. Chem. Soc. **135,** 2128 (2013).

[21] J. N. Bull, C. W. West, and J. R. R. Verlet, Chem. Sci. **7,** 5352 (2016).

[22] T. Debnath, M. S. B. M. Yusof, P. J. Low, and Z.-H. Loh, Nat. Commun. **10,** 2944 (2019).

[23] H. Kuramochi, S. Takeuchi, K. Yonezawa, H. Kamikubo, M. Kataoka, and T. Tahara, Nat. Chem. **9,** 660 (2017).

[24] R. F. Gunion, M. K. Gilles, M. L. Polak, and W. C. Lineberger, Int. J. Mass Spectrom. Ion Process. **117,** 601 (1992).

[25] J. B. Kim, T. I. Yacovitch, C. Hock, and D. M. Neumark, Phys. Chem. Chem. Phys. **13,** 17378 (2011).

[26] S. J. Kregel and E. Garand, J. Chem. Phys. **149,** 074309 (2018).

[27] G.-Z. Zhu, C.-H. Qian, and L.-S. Wang, J. Chem. Phys. **149,** 164301 (2018).

[28] H. T. Liu, C. G. Ning, D. L. Huang, P. D. Dau, and L. S. Wang, Angew. Chem. Int. Ed. **52,** 8976 (2013).

[29] D. H. Parker and A. T. J. B. Eppink, J. Chem. Phys. **107,** 2357 (1997).

[30] A. T. J. B. Eppink and D. H. Parker, Rev. Sci. Instrum. **68,** 3477 (1997).

[31] V. Dribinski, A. Ossadtchi, V. A. Mandelshtam, and H. Reisler, Rev. Sci. Instrum. **73,** 2634 (2002).

[32] X.-B. Wang and L.-S. Wang, Rev. Sci. Instrum. **79,** 073108 (2008).

[33] L.-S. Wang, C.-F. Ding, X.-B. Wang, and S. E. Barlow, Rev. Sci. Instrum. **70,** 1957 (1999).

[34] C. M. Choi, D. H. Choi, N. J. Kim, and J. Heo, Int. J. Mass Spectrom. **314,** 18 (2012).

[35] H. T. Liu, C. G. Ning, D. L. Huang, and L. S. Wang, Angew. Chem. Int. Ed. **53,** 2464 (2014).

[36] See the Supplemental Material at http://link.aps.org/supplemental/10.1103/PhysRevLett.125.093001 for the details of experiment, calculation, and analysis; Two-color photodetachment spectrum; Power dependent photoelectron transients; and full picosecond photoelectron spectra.

[37] J. Simons, J. Am. Chem. Soc. **103,** 3971 (1981).

[38] K. C. Woo and S. K. Kim, J. Phys. Chem. A **123,** 1529 (2019).

[39] K. Yokoyama, G. W. Leach, J. B. Kim, and W. C. Lineberger, J. Chem. Phys. **105,** 10696 (1996).

[40] K. Yokoyama, G. W. Leach, J. B. Kim, W. C. Lineberger, A. I. Boldyrev, and M. Gutowski, J. Chem. Phys. **105,** 10706 (1996).

[41] G. Chalasinski, R. A. Kendall, H. Taylor, and J. Simons, J. Phys. Chem. **92,** 3086 (1988).

[42] D. M. Neumark, K. R. Lykke, T. Andersen, and W. C. Lineberger, J. Chem. Phys. **83,** 4364 (1985).

[43] C. G. Bailey, C. E. H. Dessent, M. A. Johnson, and K. H. Bowen, J. Chem. Phys. **104,** 6976 (1996).

[44] C. S. Anstöter, G. Mensa-Bonsu, P. Nag, M. Ranković, R. Kumar T. P., A. N. Boichenko, A. V. Bochenkova, J. Fedor, and J. R. R. Verlet, Phys. Rev. Lett. **124,** 203401 (2020).

[45] G.-Z. Zhu, Y. Liu, and L.-S. Wang, Phys. Rev. Lett. **119,** 023002 (2017).

[46] J. N. Bull and J. R. R. Verlet, Sci. Adv. **3,** e1603106 (2017).